

Structure and superconductivity of $La_2PrNi_2O_7$ under pressure

Qing Tian(田清), Denghui Zhu(朱登辉), and Wei Zhang(张微)

Citation: Chin. Phys. B, 2025, 34 (**11**): 117101. DOI: 10.1088/1674-1056/adfef6
http://cpb.iphy.ac.cn; http://iopscience.iop.org/cpb

What follows is a list of articles you may be interested in

Single crystal growth and electronic structure of Fe-doped $Sr_3Ir_2O_7$

Muhammad Waqas, Bingqian Wang(王冰倩), Shuting Peng(彭舒婷), Jianchang Shen(沈建昌), Linwei Huai(淮琳崴), Xiupeng Sun(孙秀鹏), Yu Miao(缪宇), Pelda Uzun, Runqing Luan(栾润青), Zikun Feng(冯梓琨), Dai Pan(潘岱), Xinru Yong(勇欣茹), Hongxu Sun(孙鸿绪), Zhipeng Ou(欧志鹏), and Junfeng He(何俊峰)

Chin. Phys. B, 2025, 34 (**10**): 107101. DOI: 10.1088/1674-1056/adda0b

Anionic electron dimensionality and monolayer ferromagnetism in Y-Co electrides

Lu Zheng(郑璐), Zimeng Lv(吕梓萌), Xiaochen Huang(黄小琛), Zhuangfei Zhang(张壮飞), Chao Fang(房超), Yuewen Zhang(张跃文), Qianqian Wang(王倩倩), Liangchao Chen(陈良超), Xiaopeng Jia(贾晓鹏), Biao Wan(万彪), and Huiyang Gou(缑慧阳)

Chin. Phys. B, 2025, 34 (**9**): 097105. DOI: 10.1088/1674-1056/adf82f

Strain tuning of charge density wave and Mott-insulating states in monolayer VTe_2

Wenqian Tu(涂文倩), Run Lv(吕润), Dingfu Shao(邵定夫), Yuping Sun(孙玉平), and Wenjian Lu(鲁文建)

Chin. Phys. B, 2025, 34 (**9**): 097103. DOI: 10.1088/1674-1056/ade8e0

Ground state of electron-doped *t*-*t*0-*J* model on cylinders: An investigation of finite size and boundary condition effects

Yang Shen(沈阳), Xiangjian Qian(钱湘坚), and Mingpu Qin(秦明普)

Chin. Phys. B, 2025, 34 (**8**): 087105. DOI: 10.1088/1674-1056/add00b

Nontrivial Fermi surface topology in kagome superconductor $CsTi_3Bi_5$ revealed by de Haas-van Alphen oscillation

Yuhang Zhang(张宇航), Xinwei Yi(易鑫伟), Zhen Zhao(赵振), Jiali Liu(刘家利), Aini Xu(胥艾妮), Dong Li(李栋), Zouyouwei Lu(鲁邹有为), Yue Liu(刘樾), Jihu Lu(卢佶虎), Hua Zhang(张华), Hui Chen(陈辉), Shiliang Li(李世亮), Ziyi Liu(刘子儀), Jinguang Cheng(程金光), Gang Su(苏刚), Haitao Yang(杨海涛), Xiaoli Dong(董晓莉), Hong-Jun Gao(高鸿钧), and Zhongxian Zhao(赵忠贤)

Chin. Phys. B, 2025, 34 (**7**): 077107. DOI: 10.1088/1674-1056/adc7f0

SPECIAL TOPIC — Structures and properties of materials under high pressure

Structure and superconductivity of $La_2PrNi_2O_7$ under pressure

Qing Tian(田清)[†], Denghui Zhu(朱登辉)[†], and Wei Zhang(张微)[‡]

Key Laboratory of Material Simulation Methods and Software of Ministry of Education, College of Physics, Jilin University, Changchun 130012, *China*

(Received 26 February 2025; revised manuscript received 25 August 2025; accepted manuscript online 26 August 2025)

Nickel-based superconductors have attracted great attention due to the finding of the Ruddlesden–Popper (R–P) bilayer nickelate $La_3Ni_2O_7$ with superconducting critical temperature (T_c) of 80 K at pressure above 14 GPa. Recent efforts have been devoted to the study of $La_2PrNi_2O_7$, while the detailed structure remains unclear. In this work, we explore the stability and physical properties of such an interesting system by using density functional theory and the U parameter simulation method implemented in VASP. The results show that the enthalpy of $La_2PrNi_2O_7$ is slightly larger than its parent material bilayer R–P nickelate $La_3Ni_2O_7$. The electronic structure analysis indicates that near the Fermi level, the e_g orbit of Ni dominates and strongly hybridizes with the 2p orbit of O, thereby forming a significant van Hove singularity that is conducive to superconductivity. The *Amam* phase to the $I4/mmm$ phase occurs, accompanied by an increase in the bandwidth of Ni $3d_{z^2}$ and an enhancement of the bonding–antibonding splitting (from about 0.5 eV to 1.5 eV), which leads to an increase in the density of states at the Fermi level. Our findings provide insights into the preparation and superconductivity of R–P bilayer nickelate.

Keywords: hole-doping, superconductivity

PACS: 71.15.Mb, 74.70.–b

DOI: 10.1088/1674-1056/adfef6 **CSTR:** 32038.14.CPB.adfef6

1. Introduction

The discovery of superconductivity has stimulated sustained interest in condensed matter physics owing to its transformative technological potential. While conventional superconductors are well described by phonon-mediated pairing mechanisms, the field witnessed a paradigm shift with the emergence of unconventional cuprate superconductors.[1–4] These materials exhibit extraordinary superconducting transition temperatures (T_c), reaching 135 K under ambient conditions[5] and 164 K under hydrostatic pressure.[6] The superconducting state in hole-doped cuprates originates from metallic behavior in the Cu–O σ band, culminating in d-wave pairing symmetry below T_c.[7,8] Nevertheless, fundamental aspects of the pairing mechanism remain unresolved,[3,9] particularly regarding strongly correlated electron systems where a comprehensive theoretical framework remains elusive. This knowledge gap continues to drive the search for cuprate-analogous superconducting systems.[10–12]

Nickelates, as isoelectronic analogues of cuprates,[13,14] have emerged as a strategic platform for investigating unconventional superconductivity. Infinite-layer nickelates such as $Pr_{0.82}Sr_{0.18}NiO_2$ demonstrate this potential with T_c values up to 31 K.[15] Their electronic structure shows remarkable parallels to cuprates: the Ni^{1+} valence state mimics Cu^{2+} through hole doping of the σ band,[16–18] while offering insights into unconventional superconductors' pairing mechanisms. These characteristics position nickelates as critical testbeds for elucidating high-T_c superconductivity.

Recent attention has shifted to Ruddlesden–Popper (R–P) phase nickelates with the general formula $La_{n+1}Ni_nO_{3n+1}$,[19] formed by alternating n perovskite $LaNiO_3$ layers and rock-salt LaO blocks along the c-axis. A breakthrough occurred in 2023 with the discovery of high-temperature superconductivity ($T_c \approx 80$ K at > 14 GPa) in the $n = 2$ bilayer compound $La_3Ni_2O_7$,[20–23] which is generally believed to crystallize in the orthorhombic *Amam* phase under ambient conditions. High-pressure experiments then indicated a structural phase transition above 15.0 GPa to an *Fmmm* orthorhombic configuration.[21] Recent work by Wang *et al.*[25] has further extended this understanding through temperature-dependent phase mapping, their comprehensive phase diagram identifies a new tetragonal *I4/mmm* phase stabilized near 19 GPa and 40 K, with *ab initio* analysis confirming this phase as the superconducting progenitor. While subsequent characterization revealed inherent complexities: intergrowth of $(n = 1)/(n = 3)$ phases,[26] apical oxygen vacancies,[27] and even alternating $(n = 1)/(n = 3)$ stacking sequences[28,29] — all complicating the identification of the active superconducting phase. Notably, apical oxygen vacancies exhibit detrimental effects on T_c [30,31] while the absence of diamagnetic signatures suggests possible filamentary superconductivity.[24,32] These observations underscore the necessity for phase-pure samples to disentangle intrinsic properties from structural artifacts.

[†]These authors contributed equally to this work.

[‡]Corresponding author. E-mail: zhangw_bxx@jlu.edu.cn

© 2025 Chinese Physical Society and IOP Publishing Ltd. All rights, including for text and data mining, AI training, and similar technologies, are reserved.

Significant progress was achieved through chemical substitution, yielding $La_2PrNi_2O_7$ with enhanced phase purity and a record T_c of 82.5 K at 16 GPa among nickelates.[33] This progress raises two critical questions: (1) What structural/chemical factors promote phase purity in Pr-substituted systems? (2) What electronic mechanisms underlie the enhanced superconducting response? Our work employs DFT $+U$ approaches to calculate the energy and electronic structure of this system to address these fundamental issues, and eventually found that (1) the oxygen vacancies in Pr-substituted $La_3Ni_2O_7$ are more energy-unfavorable compared with pure $La_3Ni_2O_7$, which makes it many fewer defects in $La_2PrNi_2O_7$; (2) the flat bands near the Fermi energy significantly improve the electron density of states near the Fermi level, which are responsible for the excellent superconductivity of $La_2PrNi_2O_7$.

2. Methods

In this work, the substitution of Pr was achieved using the special quasirandom structure (SQS) method implemented in the ATAT package.[34,35] This approach randomizes the atomic arrangements within a finite supercell to approximate the multisite correlation functions of an ideal disordered solid solution at the smallest possible cell size, thereby effectively modeling compositional disorder. Specifically, the La atomic sites were allowed to be randomly occupied by La, Pr species under the compositional constraint of La:Pr = 2:1. We prepared the conventional cells for *Amam* and a $\sqrt{2}\times\sqrt{2}\times 1$ supercell for the $I4/mmm$ phases of $La_3Ni_2O_7$, including four formula units. We performed structure relaxation, self-consistency, and electronic structure calculations of $La_2PrNi_2O_7$ by using density functional theory with add U parameter (DFT $+U$)[36] simulation method, which is implemented in the Vienna *ab initio* simulation package (VASP).[37] The plane-wave kinetic cut-off energy parameter of the projector augmented-wave method[38] was set to 600 eV. We employed the Perdew–Burke–Ernzerhof[39] potential with generalized gradient approximation as exchange–correlation functional. The Brillouin zone was sampled by a Γ-centered $2\pi\times 0.03$ Å^{-1} k-points grid. The structure parameters of all materials were set to experimental measurements, and we optimized both the cell's shape and atom's position until forces convergence of 0.001 eV·Å^{-1} and energy convergence of 10^{-6} eV were achieved. Since the structures of $La_2PrNi_2O_7$ and $La_3Ni_2O_7$ are similar and Ni's bonding environment in these materials is almost the same, we set the U parameter of Ni d electrons to 4 eV, according to the DFT calculation in Sun's paper.[21]

3. Results and discussion

We begin our simulation to build the structure of $La_3Ni_2O_7$ and the substituted $La_2PrNi_2O_7$. $La_2PrNi_2O_7$ has *Amam* symmetry at ambient pressure, and will transform to the $I4/mmm$ phase under pressure.[33] Then, we implemented random Pr^{3+} replacement of La^{3+} sites within *Amam* and $I4/mmm$ frameworks derived from pristine $La_3Ni_2O_7$. These structures of $La_2PrNi_2O_7$ are shown in Fig. 1.

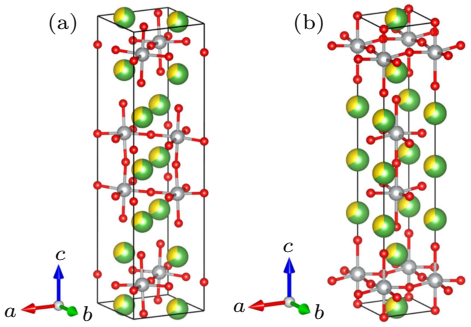


Fig. 1. The structure of $La_2PrNi_2O_7$ with different space groups. (a) The structure of the *Amam* phase at 1.6 GPa. (b) The structure of $I4/mmm$ phase at 19.6 GPa. The green and yellow spheres represent La and Pr randomly occupying the sites with an occupation ratio of La: Pr = 2:1, the green part represents La, and the yellow part represents Pr, the gray spheres represent Ni, and the red spheres represent O.

We further did structure relaxation of $La_3Ni_2O_7$ and $La_2PrNi_2O_7$, together with their enthalpy calculation. To evaluate the enthalpy variation associated with inner-apical oxygen vacancies δ, we constructed supercells by expanding the conventional *Amam* and $I4/mmm$ unit cells to contain 16 formula units. Within each supercell, the inner-apical oxygen sites were randomly sampled, and 1–4 oxygen atoms were removed to simulate different vacancy concentrations. The evolution of enthalpy versus defect ratio is summarized in Fig. 2, where the enthalpy of $\delta = 0$ was set to zero. It is no surprise that the introduction of oxygen vacancies leads to an increase in the enthalpy of both $La_3Ni_2O_{7-\delta}$ and $La_2PrNi_2O_{7-\delta}$, with Pr substitution leading to a further increase. This enhanced thermodynamic instability originates from the cooperative effects of (i) Pr-induced lattice distortions reducing structural symmetry, and (ii) vacancy-induced weakening of critical apical Ni–O bonds that stabilize the Ruddlesden–Popper framework.

Experimental studies[33] identify La:Pr = 2:1 as the critical substitution threshold for maintaining orthorhombic stability. Therefore, we suggest that $La_2PrNi_2O_7$ stays at the border of a stable state where even minor perturbations trigger phase transitions. Our analysis identifies the inner-apical oxygen sites as linchpins for structural integrity — their removal destabilizes the interlayer Ni–O bonding network essential for maintaining $n = 2$ phase coherence. Consequently, the self-limiting oxygen vacancy concentration in $La_2PrNi_2O_7$ (<0.05 vacancies/unit cell) reflects an intrinsic protection mechanism against structural collapse. Furthermore, Pr-substitution could also destabilize the $(n = 3)/(n = 1)$ phase intergrowths common in $La_3Ni_2O_7$ in the same mechanism, which effectively suppresses these interfacial defects and enhances phase purity.

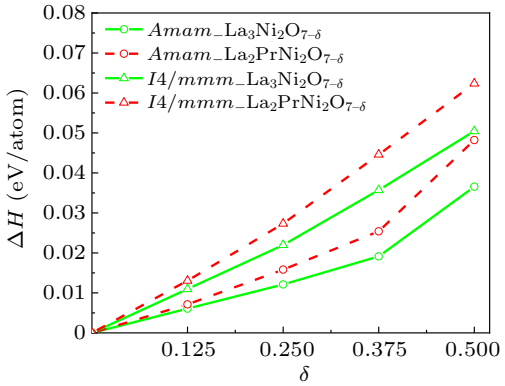


Fig. 2. The relationship between the enthalpy and the concentration of apical oxygen vacancies (δ) is shown for both $La_3Ni_2O_{-7\delta}$ and $La_2PrNi_2O_{7-\delta}$. The solid lines correspond to pristine $La_3Ni_2O_{7-\delta}$, while the dashed lines represent the Pr-substituted $La_2PrNi_2O_{7-\delta}$. The results for the *Amam* and $I4/mmm$ phases are obtained under pressures of 1.6 GPa and 19.6 GPa, respectively.

To assess the structural evolution of $La_2PrNi_2O_7$ under varying electronic correlation strengths and crystallographic symmetries, we optimized the atomic structures of both the *Amam* and $I4/mmm$ phases at 1.6 GPa and 19.6 GPa, respectively. The on-site Hubbard U values applied to the Pr 4f orbitals were set to 0 eV, 5 eV, and 6 eV. The applied U values for Pr 4f orbitals were selected according to previous studies on Pr-containing nickelates and other rare-earth systems.[40–44] The corresponding structural parameters are summarized in Table 1. For the *Amam* phase, a slight increase in the lattice constants a, b, and c is observed with increasing U, indicating a correlation-induced lattice relaxation effect. Minor changes are also found in the Ni–O bond lengths and Ni–O–Ni bond angles. In contrast, for the $I4/mmm$ phase, the lattice parameters a and b exhibit a slight contraction, accompanied by a shortening of the Ni–O bond lengths and a reduction in Ni–O–Ni bond angles as U increases. These trends suggest that the $I4/mmm$ phase hosts a more symmetric and compact NiO_6 octahedral framework, which typically favors enhanced bandwidth and covalent Ni–O bonding believed to promote superconducting tendencies in layered nickelate systems. The lattice constants vary only slightly ($\sim 0.01\%$) with different U values, which does not fundamentally alter the structural trends or the relative stability of $La_2PrNi_2O_7$.

As for the superconductivity of $La_2PrNi_2O_7$, its extraordinary property is manifested in two aspects: significant superconducting volume and superconducting temperature. While it is notable that $La_3Ni_2O_7$ exhibits filamentary superconductivity with negligible superconducting volume ($< 10\%$), since the $n = 3$ Ruddlesden–Popper analog $La_4Ni_3O_{10}$ demonstrates bulk superconductivity (volume fraction $> 80\%$),[45–47] which suggests a correlation between superconducting bulk fraction perovskite block stacking (n). However, $La_2PrNi_2O_7$ presents an apparent contradiction: despite sharing the $n = 2$ configuration with $La_3Ni_2O_7$, it achieves exceptional bulk superconductivity (97% volume fraction). This anomaly points to substitution-driven mechanisms beyond simple layer stacking.

Our calculations reveal a marginally higher enthalpy for $La_2PrNi_2O_7$ compared to its parent compound $La_3Ni_2O_7$. This thermodynamic trend arises from the random substitution of La^{3+} (ionic radius 1.95 Å) with smaller Pr^{3+} (1.85 Å), which introduces local chemical pressure and symmetry-breaking lattice distortions. Structural optimization simulations confirm these distortions, as evidenced by deviations in unit-cell parameters from ideal *Amam* and $I4/mmm$ symmetries (Table 1), contrasting with the well-preserved crystallographic symmetry in undoped $La_3Ni_2O_7$.

Since La:Pr = 2:1 is the limiting doping concentration in the regime, we propose that Pr-induced lattice distortions modify intralayer coupling within $LaNiO_3$ bilayers via Ni–O bond angle modulation. This cooperative distortion likely enhanced interlayer electronic hybridization, thereby promoting three-dimensional superconducting coherence despite identical $n = 2$ stacking.

The emergence of superconductivity is closely associated with the structural transition to the tetragonal $I4/mmm$ phase. Therefore, we carried out an in-depth investigation of the $I4/mmm$ phase at 19.6 GPa. The calculated phonon dispersion curves, shown in Fig. 3(a), exhibit no imaginary frequencies, confirming the dynamical stability of this phase. The projected phonon density of states reveals that La and Pr atoms, due to their relatively large atomic masses, primarily contribute to the low-frequency vibrations below 6 THz, while oxygen vibrations almost entirely dominate the high-frequency region above 12 THz. To further understand the bonding nature, we analyzed the crystal orbital Hamilton population (COHP)[48] of all Ni–O bonds in $La_2PrNi_2O_7$ and its parent compound $La_3Ni_2O_7$, shown in Fig. 3(b). The anti-bonding states near the Fermi level are evident, while the bonding states extend from approximately -3 eV to lower energies. At around -5.7 eV, the Ni–O bonding peak in La_3Ni_2O exhibits a larger –COHP value than that in La_2PrNi_2O, indicating a stronger Ni–O interaction in the parent compound. In contrast, the bonding peak in La_2PrNi_2O is slightly shifted to lower energy, suggesting a more stabilized bonding state. The electron localization function (ELF) analysis in Fig. 3(c) shows a high degree of electron localization around oxygen atoms, whereas the regions around Ni atoms display significant delocalization. This delocalized feature aligns with strong orbital hybridization between Ni-3d and O-2p orbitals, suggesting the formation of highly delocalized covalent Ni–O bonds. This bonding characteristic further supports the covalent metal–oxygen interaction mechanism that dominates in nickelate systems. The substitution of Pr does not significantly alter the overall ELF distribution, indicating that the bonding characteristics remain essentially unchanged.

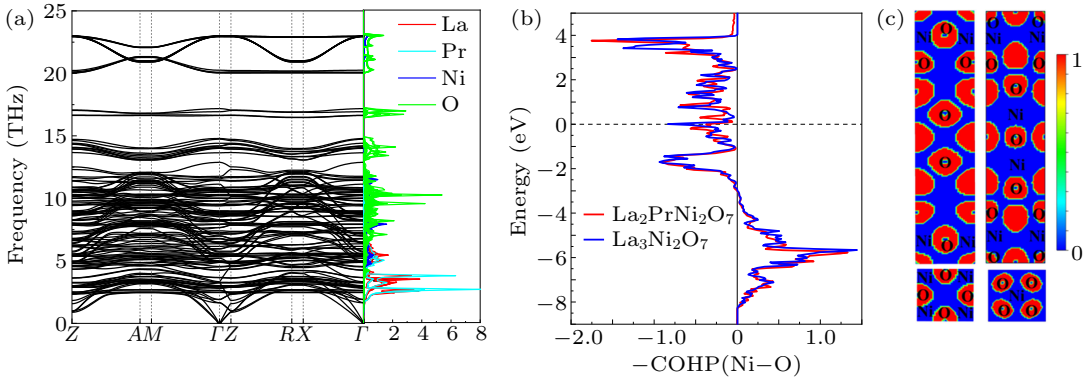


Fig. 3. The structure is in the $I4/mmm$ phase at 19.6 GPa. (a) Phonon dispersion of $La_2PrNi_2O_7$. (b) –COHP analysis of Ni–O bonds in $La_2PrNi_2O_7$ and $La_3Ni_2O_7$. (c) Electron localization function (ELF) maps of $La_3Ni_2O_7$ (left) and $La_2PrNi_2O_7$ (right), shown in the (100) (top) and (001) (bottom) planes. The color bar represents the value of ELF from 0 to 1.

Table 1. Unit cell parameters after structure relaxation of $La_3Ni_2O_7$ and $La_2PrNi_2O_7$ in *Amam* and $I4/mmm$ phases were obtained at 1.6 GPa and 19.6 GPa, respectively (with $\alpha = \gamma = 90°$). For $La_2PrNi_2O_7$, DFT+U calculations were performed with Pr U values of 5 eV and 6 eV.

Compound	Space group	Pr U (eV)	a (Å)	b (Å)	c (Å)	β (°)	Ni–O (Å)	Ni–O–Ni (°)
$La_3Ni_2O_7$	*Amam*	–	5.3842	5.5017	20.4685	90.0000	2.0071	159.9797
	$I4/mmm$	–	3.7108	3.7108	19.8307	90.0000	1.9121	180.0000
$La_2PrNi_2O_7$	*Amam*	–	5.3905	5.3221	20.4991	89.9906	1.9853	168.2853
		5	5.3912	5.3222	20.5005	89.9887	1.9899	168.2751
		6	5.3912	5.3231	20.4996	89.9902	1.9946	168.3166
	$I4/mmm$	–	3.6873	3.6662	19.8208	90.0056	1.9104	179.4439
		5	3.6869	3.6660	19.8200	90.0056	1.9103	179.4301
		6	3.6870	3.6659	19.8209	90.0058	1.9101	179.4037

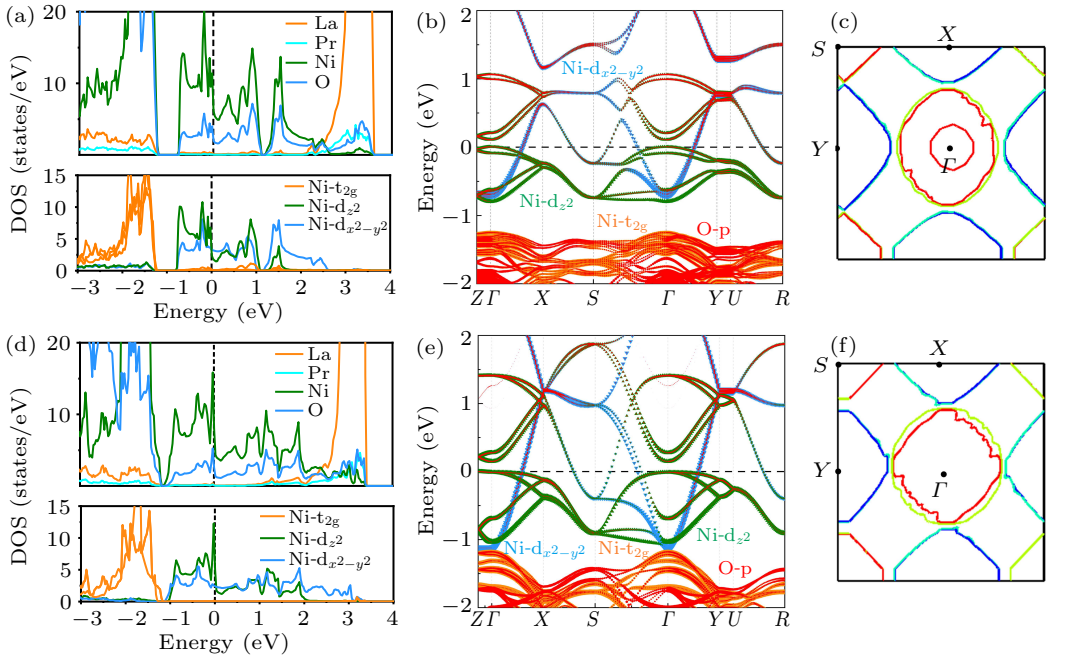


Fig. 4. Electronic structure of $La_2PrNi_2O_7$ in the *Amam* phase at 1.6 GPa (top row) and in the $I4/mmm$ phase at 19.6 GPa (bottom row). (a), (d) Orbital resolved density of states (DOS) for the La, Pr, Ni, and O atoms (upper panels) and partial density of states (PDOS) for the Ni-d_{z^2}, Ni-$d_{x^2-y^2}$, and Ni-t_{2g} states (lower panels). (b), (e) Band structure along high-symmetry lines with *Amam* phase and $I4/mmm$ phase. Colors denote the orbital character for the Ni-d_{z^2}, Ni-$d_{x^2-y^2}$, Ni-t_{2g}, and O-p orbitals. (c), (f) Two-dimensional Fermi surfaces of $La_2PrNi_2O_7$ in a Brillouin zone.

To elucidate the derivation of high-T_c in $La_2PrNi_2O_7$, we performed systematic electronic structure calculations. The electronic structures of $La_2PrNi_2O_7$ under pressures of 1.6 GPa and 19.6 GPa are shown in Fig. 4. Despite the substitution of La by Pr, the overall electronic properties remain consistent with those reported for the parent compound $La_3Ni_2O_7$.[21,25,49–53] The electronic states near the Fermi level are predominantly derived from the Ni-e_g orbitals ($3d_{z^2}$ and $3d_{x^2-y^2}$), which exhibit strong hybridization with the O-2p orbitals. The lower-lying Ni-t_{2g} states ($3d_{xy}$, $3d_{yz}$, and $3d_{xz}$) are fully occupied and exhibit notable hybridization with O-2p states approximately 1.5 eV below the Fermi level. Ac-

cording to the projected density of states (DOS), a pronounced Van Hove singularity (VHS) is present at the Fermi level. At 1.6 GPa, in the orthorhombic *Amam* phase, the Ni-3d_{z^2} states exhibit a bonding–antibonding splitting of about 0.5 eV. This behavior is consistent with the previously reported quantum coupling effects in $La_3Ni_2O_7$, where confinement within the NiO_2 bilayers leads to similar splitting.[54–56] At 19.6 GPa, in the $I4/mmm$ phase, the DOS at the Fermi level arising from Ni-3d_{z^2} orbitals is markedly enhanced. Simultaneously, the bandwidth of the Ni-3$d_{x^2-y^2}$ orbitals broadens, indicating pressure-induced enhancement of orbital dispersion. Moreover, the bonding–antibonding splitting of the 3d_{z^2} orbitals becomes more pronounced, with the energy separation increasing to about 1.5 eV, reflecting strengthened coupling between the apical O atoms and Ni-3d_{z^2} orbitals.[57] This enhanced coupling also contributes to a broader Ni-3d_{z^2} band under high pressure. The appearance of electronic flat bands along the Γ direction in the $I4/mmm$ phase and the *Amam* phase enhances the density of states at the Fermi level, leading to the formation of a VHS, which is beneficial for the emergence of superconductivity. Fermi surface calculations further reveal the nature of states near the Fermi level. In both the *Amam* and $I4/mmm$ phase, four bands cross the Fermi level, and the Ni-3d_{z^2} derived hole pockets are centered at the Γ point. Although Pr contains 4f electrons, their direct contribution to the states near the Fermi level is negligible.

4. Conclusions

Our systematic first-principles simulations investigate the structural evolution and electronic characteristics of $La_2PrNi_2O_7$. Structural relaxation reveals distinct lattice distortions in the $I4/mmm$-$La_2PrNi_2O_7$ phase compared to its parent $I4/mmm$-$La_3Ni_2O_7$ compound, attributable to isovalent substitution of La^{3+} ions by smaller Pr^{3+} cations. This substitution-induced symmetry-breaking distortion may underpin the emergent bulk superconductivity observed in the Pr-doped system.

Thermodynamic analysis demonstrates that the formation enthalpy per atom of Pr-doped $La_2PrNi_2O_7$ becomes energetically unfavorable over the $I4/mmm$-$La_3Ni_2O_7$ phase with the same apical vacancies ratio, which decreases the appearance of the defects in Pr-doped materials. Furthermore, our calculations establish the thermodynamic instability of multiphase intergrowth configurations and intrinsic defect formations in stoichiometric $La_2PrNi_2O_7$. When different Hubbard U values ($U = 0$ eV, 5 eV, 6 eV) were applied to the Pr 4f orbitals, the resulting lattice parameters showed only slight variations ($\sim 0.01\%$), indicating that the correlation effects do not fundamentally alter the structural trend.

Phonon dispersion calculations confirm the dynamical stability of the $I4/mmm$ phase at 19.6 GPa. Although the Pr substitution does not significantly affect the overall bonding characteristics, it may induce subtle distortions in the Ni–O–Ni bond angles, thereby enhancing interlayer hybridization. Electronic structure analysis reveals that the Ni-e_g orbitals dominate near the Fermi level and exhibit strong hybridization with the O-2p orbitals, leading to the formation of a pronounced VHS, which is favorable for superconductivity. Under applied pressure, the system undergoes a phase transition from *Amam* to $I4/mmm$, during which the bandwidth of the Ni-3d_{z^2} orbitals increases, and the bonding–antibonding splitting grows from about 0.5 eV to 1.5 eV, further enhancing the density of states at the Fermi level.

Acknowledgements

This work is supported by the National Key Research and Development Program of China (Grant No. 2023YFA1406103), the Education Department of Jilin Province, and Science and Technology Plan (Grant No. JJKH20211042KJ).

References

[1] Bednorz J G and Müller K A 1986 *Z. Phys. B: Condens. Matter* **64** 189
[2] Anderson P W 1987 *Science* **235** 1196
[3] Lee P A, Nagaosa N and Wen X G 2006 *Rev. Mod. Phys.* **78** 17
[4] Lechermann F 2020 *Phys. Rev. B* **101** 081110
[5] Schilling A, Cantoni M, Guo J D and Ott H R 1993 *Nature* **363** 56
[6] Gao L, Xue Y Y, Chen F, Xiong Q, Men, R L, Ramirez D, Chu C W, Eggert J H and Mao H K 1994 *Phys. Rev. B* **50** 4260
[7] Zhang F C and Rice T M 1988 *Phys. Rev. B* **37** 3759
[8] Shen Z X, Dessau D S, Wells B O, King D M, Spicer W E, Arko A J, Marshall D, Lombardo L W, Kapitulnik A, Dickinson P, Doniach S, DiCarlo J, Loeser T and Park C H 1993 *Phys. Rev. Lett.* **70** 1553
[9] Scalapino D J 2012 *Rev. Mod. Phys.* **84** 1383
[10] Maeno Y, Hashimoto H, Yoshida K, Nishizaki S, Fujita T, Bednorz J G and Lichtenberg F 1994 *Nature* **372** 532
[11] Kamihara Y, Watanabe T, Hirano M and Hosono H 2008 *J. Am. Chem. Soc.* **130** 3296
[12] Wang F and Senthil T 2011 *Phys. Rev. Lett.* **106** 136402
[13] Anisimov V I, Bukhvalov D and Rice T M 1999 *Phys. Rev. B* **59** 7901
[14] Lechermann F 2020 *Phys. Rev. B* **191** 081110
[15] Wang N N, Yang M W, Yang Z, Chen K Y, Zhang H, Zhang Q H, Zhu Z H, Uwatoko Y, Gu L, Dong X L, Sun J P, Jin K J and Cheng J G 2022 *Nat. Commun.* **13** 4367
[16] Li D, Lee K, Wang, B Y, Osada M, Crossley S, Lee H R, Cui Y, Hikita Y and Hwang H Y 2019 *Nature* **572** 624
[17] Zeng S, Tang C S, Yin X, Li C, Li M, Huang Z, Hu J X, Liu W, Omar G J, Jani H, Lim Z S, Han K, Wan D Y, Yang P, Pennycook S J, Wee A T S and Ariando A 2020 *Phys. Rev. Lett.* **125** 147003
[18] Pan G A, Segedin D F, LaBollita H, Song Q, Nica E M, Goodge B H, Pierce A T, Doyle S, Novakov S, Córdova Carrizales D, N'Diaye A T, Shafer P, Paik H, Heron J T, Mason J A, Yacoby A, Kourkoutis L F, Erten O, Brooks C M, Botana A S and Mundy J A 2022 *Nat. Mater.* **21** 160
[19] Zhang M X, Pei C Y, Wang Q, Zhao Y, Li C H, Cao W Z, Zhu S H, Wu J F and Qi Y P 2024 *J. Mater. Sci. Technol.* **185** 147
[20] Wang M, Wen H H, Wu T, Yao D X and Xiang T 2024 *Chin. Phys. Lett.* **41** 077402
[21] Sun H L, Huo M W, Hu X W, Li J Y, Liu Z J, Han Y F, Tang L Y, Mao Z Q, Yang P T, Wang B S, Cheng J G, Yao D X, Zhang G M and Wang M 2023 *Nature* **621** 493
[22] Hou J, Yang P T, Liu Z Y, Li J Y, Shan P F, Ma L, Wang G, Wang N N, Guo H Z, Sun J P, Uwatoko Y, Wang M, Zhang G M, Wang B S and Cheng J G 2023 *Chin. Phys. Lett.* **40** 117302

[23] Zhang Y N, Su D J, Huang Y N, Shan Z Y, Sun H L, Huo M W, Ye K X, Zhang J W, Yang Z H, Xu Y K, Su Y, Li R, Smidman M, Wang M, Jiao L and Yuan H Q 2024 *Nat. Phys.* **20** 1269

[24] Wang G, Wang N N, Shen X L, Hou J, Ma L, Shi L F, Ren Z A, Gu Y D, Ma H M, Yang P T, Liu Z Y, Guo H Z, Sun J P, Zhang G M, Calder S, Yan J Q, Wang B S, Uwatoko Y and Cheng J G 2024 *Phys. Rev. X* **14** 011040

[25] Wang L H, Li Y, Xie S Y, Liu F Y, Sun H L, Huang C X, Gao Y, Nakagawa T, Fu B Y, Dong B, Cao Z H, Yu R Z, Kawaguchi S I, Kadobayashi H, Wang M, Jin C Q, Mao H K and Liu H Z 2024 *J. Am. Chem. Soc.* **146** 7506

[26] Puphal P, Reiss P, Enderlein N, Wu Y M, Khaliullin G, Sundaramurthy V, Priessnitz T, Knauft M and Suthar A 2024 *Phys. Rev. Lett.* **133** 146002

[27] Dong Z H, Huo M W, Li J, Li J Y, Li P C, Sun H L, Gu L, Lu Y, Wang M, Wang Y Y and Chen Z 2024 *Nature* **630** 847

[28] Chen X L, Zhang J J, Thind A S, Sharma S, LaBollita H, Peterson G, Zheng H, Phelan D P, Botana A S, Klie R F and Mitchell J F 2024 *J. Am. Chem. Soc.* **146** 3640

[29] Wang H Z, Chen L, Rutherford A, Zhou H D and Xie W W 2024 *Inorg. Chem.* **63** 5020

[30] Liu Y B, Mei J W, Ye F, Chen W Q and Yang F 2023 *Phys. Rev. Lett.* **131** 236002

[31] Zhou Y Z, Guo J, Cai S, Sun H L, Li C Y, Zhao J Y, Wang P Y, Han J Y, Chen X T, Chen Y J, Wu Q, Ding Y, Xiang T, Mao H K and Sun L L 2025 *Matter Radiat. at Extremes* **10** 027801

[32] Sun L L, Zhou Y Z, Guo J, Cai S, Wang P Y, Zhao J Y, Han J Y, Chen X T, Wu Q, Ding Y, Xiang T and Mao H K 2024 *Evidence of filamentary superconductivity in pressurized La3Ni2O7-delta single crystals*

[33] Wang N N, Wang G, Shen X L, Hou J, Luo J, Ma X P, Yang H X, Shi L F, Dou J, Feng J, Yang J, Shi Y Q, Ren Z A, Ma H M, Yang P T, Liu Z Y, Liu Y, Zhang H, Dong X L, Wang Y X, Jiang K, Hu J P, Nagasaki S, Kitagawa K, Cheng J G 2024 *Nature* **634** 579

[34] Zunger A, Wei S H, Ferreira L G and Bernard J E 1990 *Phys. Rev. Lett.* **65** 353

[35] Van de Walle A and Ceder G 2002 *J. Phase Equilib.* **23** 348

[36] Dudarev S L, Botton G A, Savrasov S Y, Humphreys C J and Sutton A. P 1998 *Rev. B* **57** 1505

[37] Kresse G and Furthmüller J 1996 *Phys. Rev. B* **54** 11169

[38] Blochl P E 1994 *Phys. Rev. B* **50** 17953

[39] Perdew J P, Burke K and Ernzerhof M 1996 *Phys. Rev. Lett.* **77** 3865

[40] Chen W, Yuan P, Zhang S, Sun Q, Liang E and Jia Y 2012 *Physica B* **407** 1038

[41] Tran F, Schweifer J, Blaha P, Schwarz K and Novák P 2008 *Phys. Rev. B* **77** 085123

[42] Kanoun M B, Reshak A H, Kanoun-Bouayed N and Goumri-Said S 2012 *J. Magn. Magn. Mater.* **324** 1397

[43] Sayede A, Khenata R, Chahed A and Benhelal O 2013 *J. Appl. Phys.* **113** 173501

[44] Bouadjemi B, Bentata S, Abbad A, Benstaali W and Bouhafs B 2013 *Solid State Commun.* **168** 6

[45] Zhu Y H, Peng D, Zhang E K, Pan B Y, Chen X, Chen L X, Ren H F, Liu F Y, Hao Y Q, Li N N, Xing Z F, Lan F J, Han J Y, Wang J J, Jia D H, Wo H L, Gu Y Q, Gu Y M, Ji L, Wang W B, Gou H Y, Shen Y, Ying T P, Chen X L, Yang W G, Cao H B, Zheng C L, Zeng Q S, Guo J G and Zhao J 2024 *Nature* **631** 531

[46] Zhang M X, Pei C Y, Peng D, Du X, Hu W X, Cao Y T, Wang Q, Wu J F, Li Y D, Liu H Y, Wen C H P, Song J, Zhao Y, Li C H, Cao W Z, Zhu S H, Zhang Q, Yu N, Cheng P H, Zhang L L, Li Z W, Zhao J K, Chen Y L, Jin C Q, Guo H J, Wu C J, Yang F, Zeng Q S, Yan S C, Yang L X and Qi Y P 2025 *Phys. Rev. X* **15** 021005

[47] Li Q, Zhang Y J, Xiang Z N, Zhang Y H, Zhu X Y and Wen H H 2024 *Chin. Phys. Lett.* **41** 017401

[48] Dronskowski and Blöchl 1993 *J. Phys. Chem.* **97** 8617

[49] LaBollita H, Pardo V, Norman M R and Botana A S 2024 arXiv 2309.17279

[50] Liu Z, Huo M W, Li J, Li Q, Liu Y C, Dai Y M, Zhou X X, Hao J H, Lu Y, Wang M and Wen H H 2024 *Nat. Commun.* **15** 7570

[51] Li Y D, Du X, Cao Y T, Pei C Y, Zhang M X, Zhao W X, Zhai K Y, Xu R Z, Liu Z K, Li Z W, Zhao J K, Li G, Qi Y P, Guo H J, Chen Y L and Yang L X 2024 *Chin. Phys. Lett.* **41** 087402

[52] Jiang K, Wang Z Q and Zhang F C 2024 *Chin. Phys. Lett.* **41** 017402

[53] Huo Z H, Zhang P, Shi H L, Yan X C, Duan D F and Cui T 2025 *Phys. Rev. B* **111** 195118

[54] Pardo V and Pickett W E 2012 *Phys. Rev. B* **85** 045111

[55] Pardo V and Pickett W E 2010 *Phys. Rev. Lett.* **105** 266402

[56] Pardo V and Pickett W E 2011 *Phys. Rev. B* **83** 245128

[57] Jung M C, Kapeghian J, Hanson C, Pamuk B and Botana A S 2022 *Phys. Rev. B* **105** 085150